THE BELL SYSTEM TECHNICAL JOURNAL
Vol. 51, No. 8, October, 1972
Printed in U.S.A.

Optical Power Flow in Multimode Fibers

By D. GLOGE

(Manuscript received May 8, 1972)

Loss, coupling, and delay differences among the modes of multimode fibers influence their transmission characteristic in a complicated way. An approximation of the modes by a continuum leads to a comprehensive description of these interrelations. We relate the mode power distribution to the far-field output and calculate these distributions as functions of the fiber length and the input. We report measurements of the far-field distributions at various lengths of a cladded low-loss multimode fiber. A comparison of theory and experiment yields a quantitative estimate of the mode coupling involved. We associate this coupling with random irregularities of the fiber configuration and straightness, and construct a quantitative model of such irregularities.

I. INTRODUCTION

Some sources considered for use in optical communication systems have a spatially incoherent or multimode output and require overmoded fibers for efficient transmission. The fibers consist of a highly transparent core surrounded by a cladding of lower refractive index. Liquid core prototypes with losses as low as 20 dB/km have been built.[1] Solid mutimode fibers have slightly higher losses.[2] A recent study of their propagation and dispersion characteristics[3] showed a rather intricate behavior complicated by the fact that hundreds of modes could propagate simultaneously. These modes underwent a perpetual mixing process. The attenuation coefficient appeared to vary from mode to mode causing a relatively fast loss of the high-order modes.[4] An increase of delay with mode number (and fiber length) was observed as expected, but mixing and attenuation seemed to influence this relationship in a complex way.

An exact knowledge of the processes involved is of considerable interest not only to understand the sources of loss in the fiber, but in order to determine the signal distortion in long fibers. It has been predicted[5] that under certain circumstances increased mixing reduces the signal distortion (ultimately forcing all energy to propagate at an

average velocity). But it remains to be determined what actual signal improvements can be gained in practice from this effect. Previous investigations of these problems,[5,6] although suited to show the concepts involved, were limited to model studies involving relatively few modes.

In this work, we replace the modes by a continuum. This results in a relatively simple differential equation which describes the power distribution as a function of time, fiber length, and the continuous mode parameter. The differential equation can be solved rigorously for certain conditions which satisfactorily match experimental results. Explicit relations result which describe the propagation characteristics as a function of the modal coupling, attenuation, and delay coefficients. The coupling is then related to specific imperfections of the configuration or straightness of the fiber.

This paper is primarily devoted to the time-independent solution of the problem. Signal distortion and, specifically, the (baseband) impulse response of long fibers can be derived from a slight modification of the above equations and this will be done in a subsequent paper. The concept underlying our results developed from experiments with solid-core fibers[3] but, in the meantime, measurements of long liquid-core fibers[7] have proven that these fibers follow the same concept.

II. TRANSITION TO MODAL CONTINUUM

For large mode numbers, the characteristic mode parameters change so little between neighboring modes that their discrete values can be replaced by one continuous variable. Consider the two-dimensional dielectric guide–a thin film, for example–sketched in Fig. 1. We assume that the relative index difference

$$\Delta = 1 - \frac{n_c}{n} \tag{1}$$

between core index n and cladding index n_c is small compared to unity. In that case, the critical angle* for total internal reflection

$$\theta_c = \sqrt{1 - \left(\frac{n_c}{n}\right)^2} \approx \sqrt{2\Delta} \tag{2}$$

is small as well, and we can use small-angle approximations in the following relations.

Within the high-index material, the field distribution of the mth mode is essentially sinusoidal (see Fig. 1) with transverse wave number

* Defined here as the angle measured from the reflecting surface (see Fig. 1).

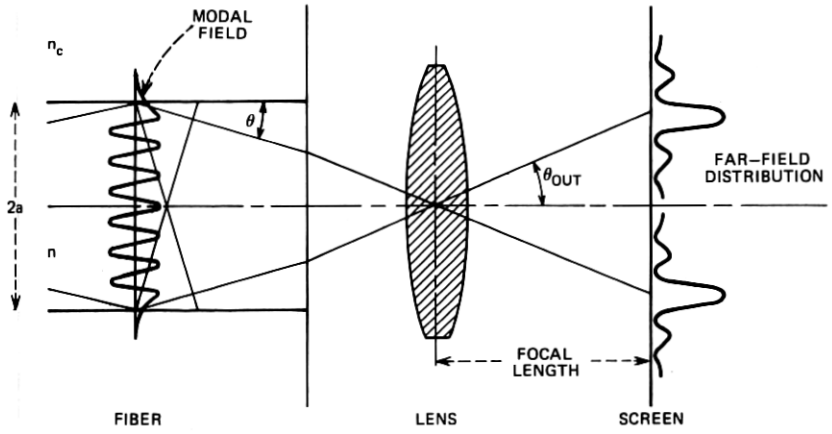

Fig. 1—Sketch to illustrate the wave nature of the modes in the dielectric slab and in the fiber.

$$u = \frac{\pi m}{2a} \tag{3}$$

where $2a$ is the guide width. If $k = 2\pi/\lambda$ is the free-space wave number, the propagation direction of a mode (i.e., its representative plane wave) follows from

$$\theta = \frac{u}{nk} = \frac{m\lambda}{4an}. \tag{4}$$

Because of Snell's law, this angle becomes

$$\theta_{out} = \frac{m\lambda}{4a} \tag{5}$$

outside of the guide. In the far field (or the focal plane of a lens), the plane waves are concentrated about the directions $+\theta_{out}$ and $-\theta_{out}$. The aperture of the guide determines the angular concentration of the two far-field "spots." If the guide width is $2a$, the spot width is of the order of λ/a.

As we learn from (4), the propagation directions of neighboring modes differ by

$$\Delta\theta = \frac{\lambda}{4an} \tag{6}$$

and hence by $\lambda/4a$ outside the guide. The modes thus form a partly

overlapping sequence of spots in the far field, ordered according to mode number. Consequently the far-field distribution represents a direct image of the modal power distribution.

The transition to the modal continuum uses a continuous angle θ instead of the discrete values (4). In this way, we arrive at a continuum of plane waves which, in the following, will be represented by rays. The power distribution $P(\theta)$, in this continuum, is obtained by replacing θ_{out} by θ in the (average) far-field power distribution.

The cylindrical configuration lacks part of the conceptual clarity associated with the plane-wave representation, but a formal similarity permits us to arrive at an equivalent ray model which is satisfactory for almost all problems related to multimode fibers. We refer again to Fig. 1, considering now a cylindrical core of radius a imbedded in cladding material. The modal field distributions are given by Bessel functions. In the case of a small index difference, there are degenerate mode pairs ($HE_{l+1,q}$ and $EH_{l-1,q}$) whose transverse mode number u is determined by the qth root of the Bessel function[8]

$$J_l(ua) = 0. \tag{7}$$

Here l is the azimuthal order number. Fig. 2, which lists a few low-order

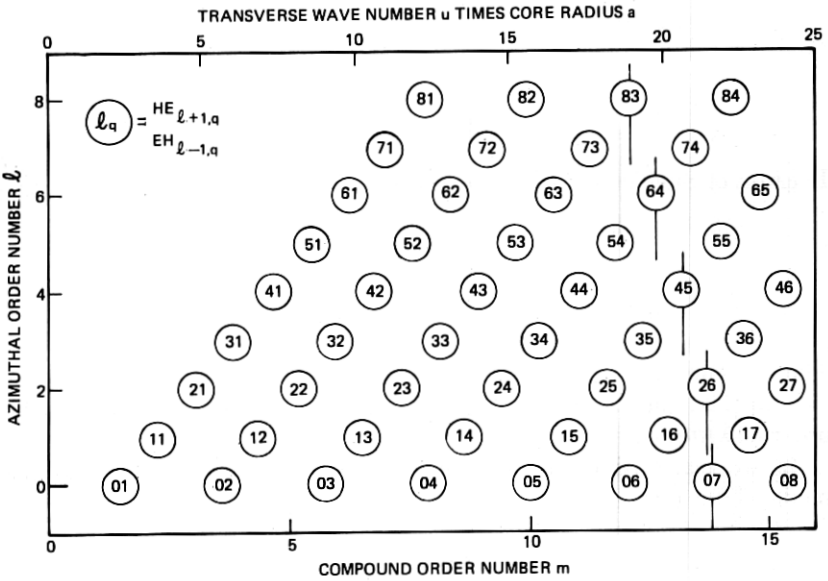

Fig. 2—The order numbers of degenerate fiber modes plotted versus ua and the effective group number $m = 2au/\pi$.

roots, has the purpose of indicating how much the exact roots deviate from the approximation

$$u = \frac{\pi}{a}\left(q + \frac{l}{2}\right), \tag{8}$$

which is to be used in the following. The group with $q + l/2 = 7$, for example, which has $ua = 22$ according to (8), is marked by vertical lines in Fig. 2.

Most problems of interest in multimode fibers (coupling, scattering loss, delay) require only the transverse wave number u for a satisfactory description of each mode. Furthermore, u can be related to a propagation angle θ and a far-field angle θ_{out}—in exact formal agreement with (4) and (5)—through an Hankel transformation of the mode field at the fiber end. This transformation shows that a mode of azimuthal order l produces l far-field spots located on a circle which is defined by the angle θ_{out} of (5). Figure 1 illustrates the situation if viewed as a meridional cross section through a cylindrical configuration.

These facts suggest a description of the cylindrical modes by a single mode number

$$m = 2q + l. \tag{9}$$

Equations (1) through (6) then obtain for the cylindrical guide as they do for the slab. The important difference is hidden in the fact that m of (9) comprises a group of modes with different q and l. As can be seen from Fig. 2, the number of possible combinations for a given m is the nearest integer below $m/2$. As mentioned earlier, every combination of q and l represents two (degenerate) modes. Consequently, each m describes a group of (approximately) m modes. In the far-field pattern, this mode group covers an annular area of "radius" θ_{out} and approximate "width" λ/a.

The transition to the continuum again converts θ to a continuous parameter. But θ is now considered as a radial variable which covers the solid angle $\pi\theta_c^2$. We have a conceptual model which consists of a continuum of rays within the cone $\pi\theta_c^2$, whereby the modal power distribution $P(\theta)$ is obtained by replacing θ_{out} in the (average) far-field power distribution by θ of (4).

To compute the total number of modes, we determine the highest possible group number $m_c = 4an\theta_c/\lambda$ by inserting θ_c into (4). If we consider also that each group has m modes; and each mode has two possible states of polarization, we have for the mode volume

$$\sum_{m=1}^{m_c} 2m = \left(\frac{4an}{\lambda}\right)^2 2\Delta. \tag{10}$$

A comparison with the more accurate number $(2\pi an/\lambda)^2\Delta$ from Ref. 8 gives an indication of the quality of the approximations used here.

III. POWER FLOW EQUATION

For the sake of simplicity, the following derivation is based on a model which seems to have limited validity at first glance. We assume that mode coupling takes place only between next neighbors. It will become apparent later that the error involved in this approximation is small if other modes couple also, but the coupling strength decreases sufficiently fast with the mode spacing. There is experimental evidence[3,7] that a mechanism of this kind is indeed present in real multimode fibers. Fig. 3, for example, shows a measurement performed with the solid-core multimode fiber mentioned previously.[2,3] The core diameter was 55 μm, the relative index difference $\Delta = 0.0046$, and the nominal loss 33 dB/km. About 700 modes could propagate. By injecting a very narrow cone of light (through an index-matching cell), we excited about 150 of the low-order modes. This was measured by scanning the far-field of the output after 30 cm of fiber. Similar measurements with longer fibers revealed a slow but steady increase in the number of excited modes (the angular far-field width) with fiber length. This slow increase is considered as strong evidence of a power exchange which favors near neighbors and decreases rapidly with mode spacing.

To simplify matters, let us again consider the two-dimensional case first. As long as the coupling mechanism is a statistical process, we can

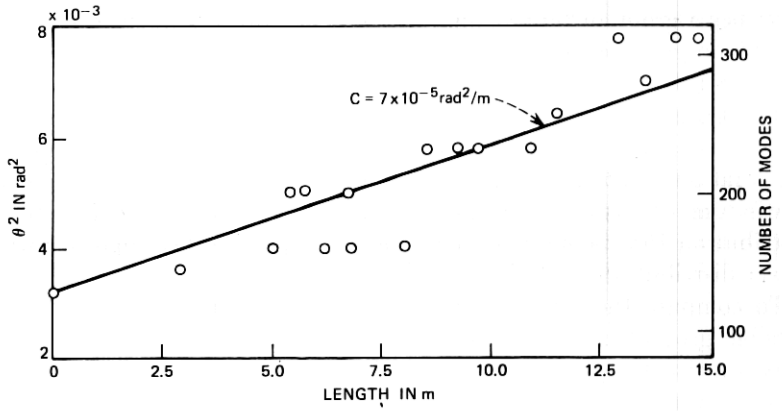

Fig. 3—The increase of mode volume with fiber length measured in a multimode fiber which propagated 700 modes.

ignore the individual mode fields and obtain the power distribution directly from some form of power rate equations.[9] These consider the variation dP_m in the power P_m of the mth mode along a guide increment dz. In the time-invariant case, the variation dP_m has two causes: (*i*) dissipation and loss (scattering) to the outside, which we comprise in a term $-\alpha_m P_m dz$; (*ii*) coupling to other modes. Our simplified model assumes coupling between neighboring modes only. Thus, if d_m is the coupling coefficient between the modes of order $m + 1$ and m, we have

$$\frac{dP_m}{dz} = -\alpha_m P_m + d_m(P_{m+1} - P_m) + d_{m-1}(P_{m-1} - P_m). \tag{11}$$

The transition to the continuum requires power differences to be replaced by differentials. Especially, we set

$$\frac{P_{m+1} - P_m}{\theta_{m+1} - \theta_m} = \frac{dP_m}{d\theta}. \tag{12}$$

With $\theta_m - \theta_{m-1} = \Delta\theta$ from (6), we can rewrite (11) in the form

$$\frac{dP_m}{dz} = -\alpha_m P_m + \Delta\theta\left(d_m \frac{dP_m}{d\theta} - d_{m-1} \frac{dP_{m-1}}{d\theta}\right). \tag{13}$$

The remaining difference requires an analogous transition

$$d_m \frac{dP_m}{d\theta} - d_{m-1} \frac{dP_{m-1}}{d\theta} = \Delta\theta \frac{d}{d\theta}\left(d_m \frac{dP_m}{d\theta}\right). \tag{14}$$

After replacing the index m everywhere by a functional dependence of θ, we finally obtain the power flow equation

$$\frac{\partial P}{\partial z} = -\alpha(\theta)P + (\Delta\theta)^2 \frac{\partial}{\partial\theta}\left[d(\theta) \frac{\partial P}{\partial\theta}\right]. \tag{15}$$

In the cylindrical case, the index m stands for a group of m modes. To obtain the power equation for the mth mode group, we must therefore sum (11) over all m members. The coefficients α_m and d_m depend only on m, and hence are the same for all group members.[10] However, the coupling to the lower group $(m - 1)$ can occur only between $m - 1$ members. Thus

$$m \frac{dP_m}{dz} = -m\alpha_m P_m + m d_m(P_{m+1} - P_m) + (m - 1)d_{m-1}(P_{m-1} - P_m). \tag{16}$$

Using (12) and a transition analogous to (14), we obtain

$$\frac{\partial P}{\partial z} = -\alpha_m P_m + (\Delta\theta)^2 \frac{1}{m} \frac{\partial}{\partial \theta} \left(m d_m \frac{\partial P_m}{\partial \theta} \right). \tag{17}$$

With the help of (4) this finally leads to

$$\frac{\partial P}{\partial z} = -\alpha(\theta) P + (\Delta\theta)^2 \frac{1}{\theta} \frac{\partial}{\partial \theta} \left[\theta d(\theta) \frac{\partial P}{\partial \theta} \right]. \tag{18}$$

Because of the symmetry involved, we can expand α in the form

$$\alpha(\theta) = \alpha_o + A\theta^2 + \cdots,$$

where α_o comprises loss common to all modes. A loss of this kind can later be accounted for by multiplying the final solution by a term $\exp(-\alpha_o z)$. For the moment, we ignore this part of the loss. Among the higher orders, the term $A\theta^2$ is the most important one, because it essentially comprises the loss caused at the core-cladding interface. This is so because the power density at the interface increases quadratically with the transverse wave number u of a certain mode[8] and hence quadratically with θ. In the following, we retain only this important term.

The coupling coefficient $d(\theta)$ requires the same expansion. Its zero-order term is essential and cannot be accounted for later on. Although no estimates exist on the magnitude of other terms, the following derivation merely retains this first term. Its physical significance will become clearer as we proceed. Thus with

$$d(\theta) = d_o \tag{19}$$

or

$$D = (\Delta\theta)^2 d_o = \left(\frac{\lambda}{4an} \right)^2 d_o, \tag{20}$$

we can write (15) and (18) in the form

$$\frac{\partial P}{\partial z} = -A\theta^2 P + D \frac{\partial^2 P}{\partial \theta^2} \quad \text{for the slab,} \tag{21}$$

and

$$\frac{\partial P}{\partial z} = -A\theta^2 P + \frac{D}{\theta} \frac{\partial}{\partial \theta} \left(\theta \frac{\partial P}{\partial \theta} \right) \quad \text{for the fiber.} \tag{22}$$

The form of the last terms in (21) and (22) identifies next-neighbor mode coupling as a diffusion process in the continuum.

Solutions that are independent of z can be obtained from the substitution

$$P = Qe^{-\gamma z}, \tag{23}$$

where γ denotes a (power) attenuation constant related to the "steady-state" solution Q. Equations (21) and (22) take the form

$$D\frac{\partial^2 Q}{\partial \theta^2} = (A\theta^2 - \gamma)Q \quad \text{for the slab,} \tag{24}$$

and

$$\frac{D}{\theta}\frac{\partial}{\partial \theta}\left(\theta \frac{\partial Q}{\partial \theta}\right) = (A\theta^2 - \gamma)Q \quad \text{for the fiber.} \tag{25}$$

The first of these equations is satisfied by the Hermite-Gaussian, and the second by the Laguerre-Gaussian polynomials; both are well known from the theory of the open resonator. The attenuation parameters γ associated with each of these solutions increase with the order of the polynomial.

Both for the slab and the fiber, the solutions of least loss have the form

$$\exp(-\theta^2/\Theta_\infty^2) \tag{26}$$

with

$$\Theta_\infty = (4D/A)^{\frac{1}{4}}. \tag{27}$$

The power loss associated with this distribution is

$$\gamma_\infty = (AD)^{\frac{1}{2}} \qquad \text{for the slab,} \tag{28}$$

and

$$\gamma_\infty = 2(AD)^{\frac{1}{2}} \qquad \text{for the fiber.} \tag{29}$$

The distribution (26) constitutes an optimum balance between the loss in high-order modes and the steady outflow of power into those modes through coupling. It is assumed, of course, that the critical angle θ_c is so large compared to Θ_∞, that the steady-state distribution (26) is not significantly influenced by the boundary relations at $\theta = \theta_c$. If this is not the case, the solutions of (24) and (25) have to take these boundary relations into account.

IV. BUILD-UP FROM GAUSSIAN INPUT

Any z-dependent solution of (21) or (22) can of course be constructed from the infinite set of solutions of (24) and (25). But in the case of the fiber, there is a certain interest in special solutions which have an

arbitrary Gaussian input

$$P_{in} = P_o \exp [-\theta^2/\Theta_0^2] \tag{30}$$

as initial condition. This is because it is convenient to study multimode fibers by using a Gaussian laser beam for excitation. A high-power lens converts this beam into the angular Gaussian distribution (30). By observing the change in $P(\theta)$ with fiber length, and the loss as a function of various (Gaussian) input distributions, one obtains valuable information on the power flow in the fiber.

Since both the input and the steady-state are Gaussian, it is reasonable to try the solution

$$P = f(z) \exp [-\theta^2/\Theta^2(z)]. \tag{31}$$

Although this approach is useful both for the two- and the three-dimensional configuration, we shall concentrate in the following on the fiber only. Introducing (31) into (22) yields the two differential equations

$$d\Theta/dz = -\frac{A}{2}\Theta^3 + 2D/\Theta \tag{32}$$

and

$$df/dz = -4Df/\Theta^2. \tag{33}$$

We can solve the first of these equations for Θ and obtain

$$\Theta^2 = \Theta_\infty^2 \begin{Bmatrix} \tanh \gamma_\infty(z + z_o) \\ \coth \gamma_\infty(z + z_o) \end{Bmatrix} \tag{34}$$

with the steady-state parameters Θ_∞ and γ_∞ from (27) and (29). The choice of tanh or coth and the coefficient z_o are determined by the initial conditions. Eq. (33) can be solved with the help of (34) and yields

$$f = f_o \begin{Bmatrix} \sinh \gamma_\infty(z + z_o) \\ \cosh \gamma_\infty(z + z_o) \end{Bmatrix}. \tag{35}$$

A Gaussian input stays indeed Gaussian, its width approaching monotonically that of the steady state. The transition function is the hyperbolic tangent if the input width is smaller than the steady-state width and the hyperbolic cotangent in the opposite case. For the initial conditions (30), the solutions (34) and (35) can be written in the form

$$\Theta^2(z) = \Theta_\infty^2 \frac{\Theta_o^2 + \Theta_\infty^2 \tanh \gamma_\infty z}{\Theta_\infty^2 + \Theta_o^2 \tanh \gamma_\infty z} \tag{36}$$

and

$$f(z) = \frac{P_o\Theta_o^2}{\Theta_\infty^2 \sinh \gamma_\infty z + \Theta_o^2 \cosh \gamma_\infty z}. \tag{37}$$

To obtain the total power in the guide, $P(\theta)$ must be integrated over all angles up to θ_c. If we assume, as previously, that $P(\theta)$ is sufficiently small at the critical angle θ_c and beyond, we can extend the integration to infinity. With (31), the total power is

$$2\pi \int_0^\infty P(\theta)\theta d\theta = \pi f \Theta^2. \tag{38}$$

The power loss per unit length is consequently

$$\gamma(z) = -\frac{1}{f\Theta^2}\frac{d}{dz}(f\Theta^2). \tag{39}$$

By using the differentials $d\Theta/dz$ and df/dz from (32) and (33), we obtain

$$\gamma(z) = A\,\Theta^2(z). \tag{40}$$

With (27) and (29) this can also be written in the form

$$\frac{\gamma(z)}{\gamma_\infty} = \frac{\Theta^2(z)}{\Theta_\infty^2}. \tag{41}$$

The ratio (41) is plotted in Fig. 4 versus the fiber length for some specific input conditions. The plot illustrates the loss, the solid angle covered by the fiber output and, since this is proportional to the mode volume, also the number of modes propagating in the fiber.

If the measured width $\Theta(z)$ is small compared to the steady-state width Θ_∞, we can approximate (36) by

$$\Theta^2 = \Theta_\infty^2\gamma_\infty z + \Theta_o^2. \tag{42}$$

In this case, because of (27) and (29), $\Theta^2(z)$ is a straight line with the slope

$$\Theta_\infty^2\gamma_\infty = 4D. \tag{43}$$

Thus measuring $\Theta^2(z)$ under these conditions yields directly the coupling parameter D. The approximate linear increase of the data in Fig. 3 is an indication of the validity of (42). A straight-line approximation of the measured data yields

$$D = 7 \cdot 10^{-5}\ \text{rad}^2/\text{m}. \tag{44}$$

This value represents a first approximation for the zero-order coupling

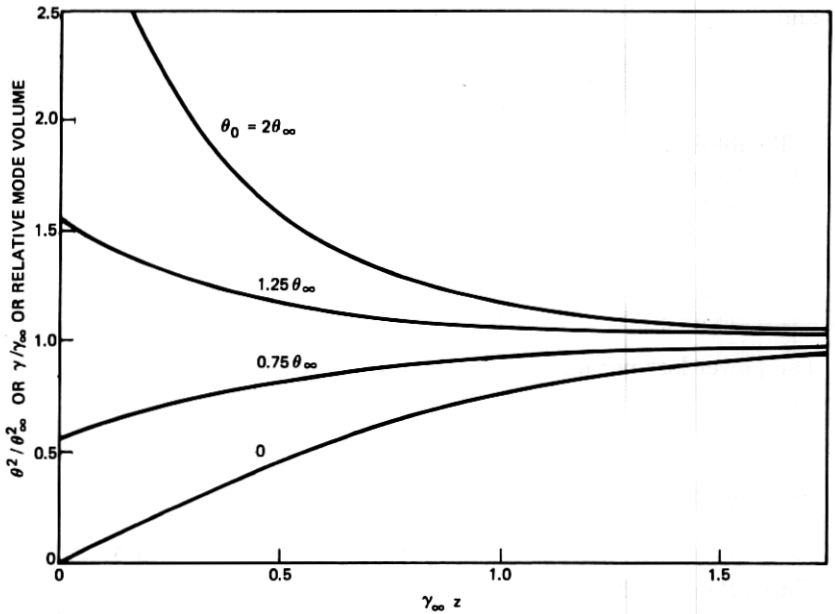

Fig. 4—Calculated increase of mode volume and loss with fiber length. The data are related to the steady-state values.

coefficient d_o which, because of (20), becomes $d_o = 16\ \mathrm{m}^{-1}$ at the measuring conditions ($a = 50\ \mu\mathrm{m}$, $\lambda = 0.63\ \mu\mathrm{m}$). The range of the measured data is not sufficient to draw any conclusions on the size of higher-order coefficients in $d(\theta)$.

V. TWO SOURCES OF COUPLING

Marcuse[10] has studied a dielectric slab guide with slightly distorted interfaces. He finds that two modes are coupled if the surface imperfections comprise a component of wavelength Λ that coincides with the "beat wavelength" between the two modes. The beat wavelength is the distance in which the phase difference between two modes increases to 2π. It can be calculated from the wave number

$$\beta_m = (k^2n^2 - u^2)^{\frac{1}{2}} \approx kn - \frac{1}{2}\frac{u^2}{kn} \tag{45}$$

of the mth mode. With u from (3), we obtain for two neighboring modes of order m and $m + 1$,

$$\Lambda = \frac{2\pi}{\beta_m - \beta_{m+1}} = \frac{4a}{\theta}. \tag{46}$$

This is also the distance that a ray of angle θ requires to complete a zigzag period in a slab of width $2a$.

To describe the distorted slab walls, let us define a "power" spectrum $\phi(1/\Lambda)$ of the (random) deviations $\delta(z)$ from ideally straight interfaces. If the irregularities of both walls are uncorrelated, the coupling coefficient $d(\theta)$ between adjacent modes is[10]

$$d = \frac{1}{2}\left(\frac{nk}{a}\right)^2 \theta^4 \phi\left(\frac{\theta}{4a}\right). \tag{47}$$

Using this relation and (20), we can calculate the spectrum associated with the measured coupling parameter D of (44): The result

$$\phi\left(\frac{1}{\Lambda}\right) = \frac{D\Lambda^4}{32\pi^2} \tag{48}$$

suggests a decrease of ϕ with the fourth power of the (spatial) frequency $1/\Lambda$.

This result permits us to estimate the coupling among nonadjacent modes. As is evident from (45) and (46), modes which differ by a small number r have the beat wavelength $4ra/\theta$. Because of (48), coupling among such modes decreases with the fourth power of their order difference. It is this rapid decrease which permitted us to neglect all coupling except that between next-neighbors in (11). The error involved in this approximation can be estimated for the case that the power distribution $P(\theta)$ changes slowly within $r\Delta\theta$. In that case,

$$\frac{P_{m+r} - P_m}{\theta_{m+r} - \theta_m} \approx \frac{dP}{d\theta} \quad \text{for} \quad r \ll m. \tag{49}$$

The transition from (11) to (15) then allows us to lump the coupling of all modes from m to $m + r$ in the coefficient $d_m = d(\theta)$ which assumes the form

$$d \sum_{r=1}^{\infty} \frac{1}{r^4} = \frac{\pi^4}{90} d \approx 1.08d. \tag{50}$$

This suggests that the relative error in our approximation is as small as 8 percent.

Random bends in the guide are another source of coupling. This problem has been studied by tracing rays through a randomly curved slab guide.[11] The result relates the statistics of the ray angle θ to the

"power spectrum" $C(1/\Lambda)$ of the curvature components. Reference 11 demonstrates that components of wavelength Λ predominantly influence rays with the same zigzag wavelength. For a short guide length z, the probability distribution of the ray angle θ is found to have a variance which increases as

$$\sigma^2(z) = \frac{8}{\pi^2} zC\left(\frac{\theta}{4a}\right) + \sigma_o^2 \tag{51}$$

where σ_o^2 is the variance at the input.[11] These results presuppose Gaussian statistics, for which the probability to find a ray at θ has the form $\exp(-\theta^2/2\sigma^2)$.

Let us compare this distribution to the distribution

$$P(\theta) = \exp[-\theta^2/\Theta^2]$$

of (31). For negligible mode attenuation, the width of this Gaussian is given by the simple relation (42). Like the variance of (51), it grows linearly with length. A comparison of the growth factors involved must take the factor 2 into account which enters because of the definition of the variance. This leads to the relation

$$C\left(\frac{1}{\Lambda}\right) = \frac{\pi^2}{4} D. \tag{52}$$

To compare this result with ϕ of (48), let us consider correlated deviations of the form $\delta \sin(2\pi z/\Lambda)$ at both walls. Twofold differentiation with respect to z transforms this into a curvature component of the form $(2\pi/\Lambda)^2\delta \sin(2\pi z/\Lambda)$. Accordingly, we can relate the curvature spectrum to a spectrum of (correlated) irregularities

$$\phi_c\left(\frac{1}{\Lambda}\right) = (\Lambda/2\pi)^4 C. \tag{53}$$

This result transforms (52) into

$$\phi_c\left(\frac{1}{\Lambda}\right) = \frac{D\Lambda^4}{64\pi^2}. \tag{54}$$

The factor 2 which distinguishes this result from (48) results from the correlation of the wall deviations assumed in (53) contrary to (48);[10] to represent a curved slab, the deviations must be equal and in phase.

Irregularities of this kind couple only modes which differ by an odd order number $r = 1, 3, \cdots$. Coupling across even numbers results from irregularities in anti-phase or—in the case of the fiber—from irregularities of at least twofold cross-sectional symmetry. Specific parts of the spectrum $\phi(1/\Lambda)$ are likely to be dominated by certain kinds of irregularities.

The region of interest is determined by $\Lambda = 4a/\theta$ and was in our case between $\Lambda = 1$ and 10 mm. Since these lengths are significantly larger than the core diameter (150 μm), we believe that bends were the dominant source of coupling. The following example therefore uses the relation (52) for a quantitative estimate of the irregularities involved. Although (52) applies specifically to the slab model, we shall combine it with the fiber data (44), confident that this will illustrate at least the orders of magnitude involved.

To obtain a more tangible description of the random curvature, we assume it to be composed of randomly distributed singular deviations of the kind illustrated in Fig. 5a. We model these deviations by single-period sinewaves of the form $\delta \sin (2\pi z/\Lambda)$. Essentially, only those with a width larger than $\Lambda/2$ contribute to the curvature spectrum at Λ. If there are η of those per unit length, the curvature spectrum has approximately the value[11]

$$C = 8\pi^4 \eta \, \delta^2/\Lambda^2 \tag{55}$$

in the vicinity of Λ. Because of (52)

$$\eta \delta^2 = \frac{\Lambda^2 D}{32\pi^2}. \tag{56}$$

Fig. 5b evaluates this relation for the case of the fiber measured. Plotted is the density η versus the amplitude δ for ray periods (and angles) of interest. For example, an average of 1000 singular irregularities per meter would account for the coupling measured, if their magnitudes obeyed the relation $\delta = 15 \cdot 10^{-6} \Lambda$. That would mean that the magnitude of the irregularities increases linearly with their length reaching a value of 15 nm at $\Lambda = 1$ mm.

VI. CONCLUSIONS

A comprehensive description of a multimode fiber by one differential equation is possible, if the modes are approximated by a continuum. Under certain realistic conditions, this equation has a rigorous solution. We calculate here the far-field output distribution as a function of fiber length and compare this to experiments performed with a low-loss multimode fiber. We find neighboring modes to be coupled by an average 1.6 percent per mm. Coupling among other modes seems to be at least an order of magnitude less.

Among the possible sources of coupling taken into consideration, we believe random bends to be the most likely. In this case, the curvature

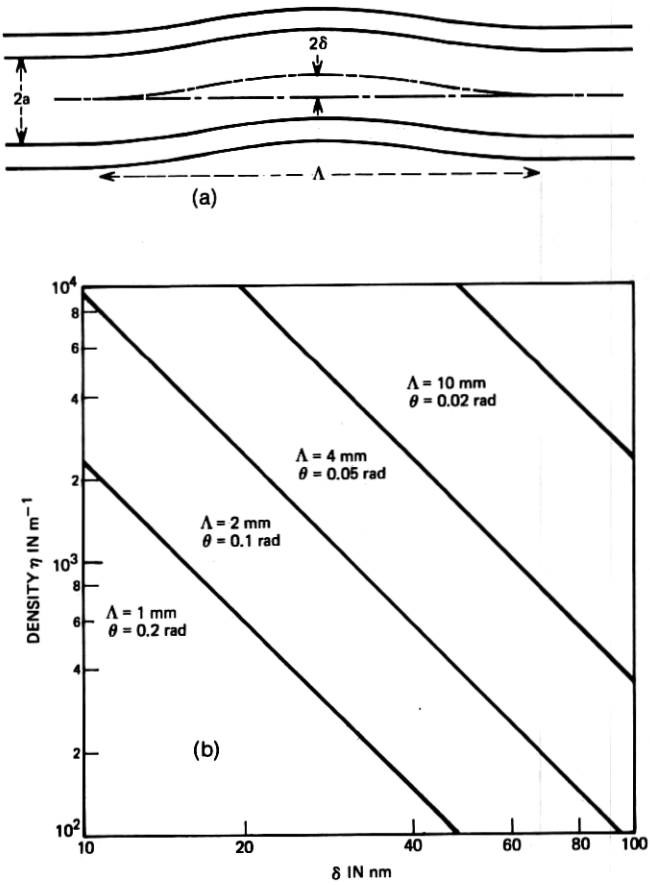

Fig. 5—Deviations from straightness as indicated in (a) account for the coupling measured, if their density η, and magnitude δ are related to their length Λ as plotted in (b).

spectrum has a value of $2 \cdot 10^{-7}$ mm^{-1} in the region of spatial ferquencies between 0.1 and 1 mm^{-1}. Another equivalent description of this result is by small hump-shaped deviations from straightness—on the average 1000 of them per meter—the magnitude of which increases proportionally to their length and is about 15 nm for a length of 1 mm.

The theory derived here can be modified to include the velocity differences among the modes and, in this way, to describe the impulse response in the presence of coupling and loss. This will be the subject of another paper.

VII. ACKNOWLEDGMENT

The experiment was performed together with E. L. Chinnock whose skillful cooperation is gratefully acknowledged.

REFERENCES

1. Stone, J., "Optical Transmission Loss in Liquid-Core Hollow Fibers," Topical Meeting on Integrated Optics—Guided Waves, Materials, and Devices, Las Vegas, Nevada, February 7–10, 1972.
2. Manufactured by Corning Glass Works, Corning, New York.
3. Gloge, D., et al., "Dispersion in a Low-Loss Multimode Fiber Measured at Three Wavelengths," Topical Meeting on Integrated Optics—Guided Waves, Materials and Devices, Las Vegas, Nevada, February 7–10, 1972.
4. Gloge, D., et al., "Picosecond Pulse Distortion in Optical Fibers," IEEE J. Quantum Elec., *QE-8* (1972), pp. 217–221.
5. Personick, S. D., "Time Dispersion in Dielectric Waveguides," B.S.T.J., *50*, No. 3 (March 1971), pp. 843–859.
6. Marcuse, D., "Pulse Propagation in Multimode Dielectric Waveguides," B.S.T.J., *51*, No. 6 (July–August 1972), pp. 1199–1232.
7. Gloge, D., Chinnock, E. L., and Stone, J., "Dispersion Measurements in Liquid-Core Fibers," unpublished work.
8. Gloge, D., "Weakly Guiding Fibers," Appl. Opt., *10*, 1971, pp. 2252–2258.
9. Marcuse, D., "Derivation of Coupled Power Equations," B.S.T.J., *51*, No. 1 (January 1972), pp. 229–237.
10. Marcuse, D., "Mode Conversion Caused by Surface Imperfections of a Dielectric Slab Waveguide," B.S.T.J., *48*, No. 10 (December 1969), pp. 3187–3215.
11. Gloge, D., "Bending Loss in Multimode Fibers With Graded and Ungraded Core Index," to appear in Applied Optics.